



Cold Climates, Complex Hydrology: Can A Land Surface Model Accurately Simulate Deep Percolation?

Alireza Amani¹, Marie-Amélie Boucher¹, Alexandre R. Cabral¹, Vincent Vionnet², and Étienne Gaborit²

¹Department of Civil and Building Engineering, Université de Sherbrooke, Sherbrooke, Quebec, Canada

²Environmental Numerical Weather Prediction Research, Environment and Climate Change Canada, Dorval, Quebec, Canada

Correspondence: Alireza Amani (Alireza.Amani@usherbrooke.ca)

Abstract. Cold regions present unique challenges for land surface models simulating deep percolation or potential groundwater recharge. Previous model evaluation efforts often overlooked these regions and did not account for various sources of uncertainties influencing model performance and its evaluation. This work addresses these limitations using high-resolution integrated lysimeter measurements to assess the performance of the SVS land surface model in a cold climate. SVS showed promise in the simulation of snowmelt and rainfall-driven deep percolation events. It also simulated daily snow depth well, with a correlation coefficient (r) greater than 0.94 and a mean-bias-error (MBE) smaller than 3.0 cm for most of the simulation period. The newly implemented soil-freezing scheme reasonably simulated the near-surface soil temperature ($r = 0.89$) with a slight cold bias (MBE = -0.8°C). However, the model's inability to represent frozen soil infiltration and preferential flow resulted in a significant underestimation of percolation ($r: 0.35$, MBE: $-0.8\text{ mm}\cdot\text{day}^{-1}$) and near-surface soil moisture during cold months (MBE: $-0.058\text{ m}^3\cdot\text{m}^{-3}$). Those findings highlight the importance of a comprehensive model evaluation for improving deep percolation modeling in cold regions. Such improvements can lead to more informed decision-making regarding groundwater resource management in a changing climate.

1 Introduction

Groundwater is a vital resource facing increasing pressure globally, with declining recharge rates threatening its sustainability (Noori et al., 2023; Wada et al., 2010; Gleeson et al., 2012; Dalin et al., 2017; Nygren et al., 2021). Physics-based numerical models are important for estimating (potential) groundwater recharge or deep percolation (Cao et al., 2016; Dash et al., 2019). However, a key question remains: Can we trust these models, particularly in cold environments where water and energy fluxes are intricately linked (Wheater et al., 2022; Cordeiro et al., 2017; Pomeroy et al., 2022)? Physics-based numerical models such as land surface models (LSMs) can simulate these complex interactions (Arora et al., 2023; Fisher and Koven, 2020). LSMs can explore 'what if' scenarios, enhance understanding of physical processes, and provide process-based predictions with explanatory power (Willcox et al., 2021). For example, they help quantify how changing precipitation patterns impact groundwater recharge (Trenberth, 2011; Wu et al., 2020). This is particularly important in regions where fluctuations of groundwater resources heavily influence ecosystem water availability (Huang et al., 2019; Orellana et al., 2012). Beyond natural systems, LSMs can guide the design of landfill final covers. Designers can optimize the covers by simulating how prospective covers



25 interact with local hydrometeorological conditions (Ho et al., 2004) to minimize leachate production. This pre-construction analysis saves time and resources.

Robust process-based model evaluation is integral to assessing a model's 'fit-for-purpose' (Beven and Young, 2013) of LSMs and identifying areas for targeted improvement (Wilson et al., 2021). Evaluating deep percolation simulations goes beyond assessing the final output. Examining how well the model represents the key physical processes influencing deep
30 percolation is crucial. Several factors complicate such evaluations. First, direct measurements of deep percolation are difficult, costly, and scarce (Li and Shao, 2014). But they substantially minimize errors compared to indirect methods and can be used to calibrate them (Benson et al., 2001; Meissner et al., 2008; Ouédraogo et al., 2022). Indirect methods such as those using soil water content data are critically limited in accounting for deep percolation due to preferential flow (Khire et al., 1997; Benson et al., 2001). Second, pinpointing limitations in models' structure and parameterization requires accounting for uncertainties
35 in forcing data and parameter values (Oreskes et al., 1994). Finally, choosing an appropriate temporal resolution for model evaluation is crucial. High-resolution observations, such as those obtainable from lysimeters at daily or hourly time steps, help identify the strengths and weaknesses of how specific processes are represented in the model. Coarse-resolution (annual or total) evaluation may hide compensating errors in simulating different processes.

We performed a literature search (Scopus) to assess previous model evaluation studies comparing simulated deep percolation
40 with lysimeter measurements. The search yielded 57 articles, published between 1998 and 2024. Figure 1-c maps the location of these case studies. Figures 1-a and 1-b provide the frequency of climate types (Köppen classification (Peel et al., 2007)) and evaluation time scales, respectively. Most studies evaluated models' deep percolation at coarser-than-daily resolutions. HYDRUS (Simunek et al., 2005) was the most common model (28 out of 57), followed by UNSAT-H (Fayer, 2000). Only two LSMs were evaluated: ISBA (Sobaga et al., 2023) and HTSVS (Mölders et al., 2003). A key finding is the lack of attention to
45 strategies accounting for different sources of uncertainty. None of the studies accounted for the uncertainty in forcing data and observations, and only four accounted for parameter uncertainty (Schwemmler and Weiler, 2024; Selim et al., 2023; Graham et al., 2018; Ogorzalek et al., 2008). This is an important limitation, particularly in the context of cold regions, because small biases in forcing data can significantly impact process simulations (Wheater et al., 2022). Snow and soil freezing processes were rarely considered (only one study analyzed their influence (Mölders et al., 2003)). This is likely due to the geographical
50 distribution of the case studies (limited snow influence) and model limitations. In some instances, the latter necessitated the removal of snowy periods from analysis (Mijares and Khire, 2012) or simplifying approaches like a degree-day snowmelt constant (Stumpp et al., 2012).

This study aims to improve deep percolation simulation, specifically for cold environments, through a comprehensive evaluation of the Soil, Vegetation, and Snow (SVS, Alavi et al. (2016); Husain et al. (2016)) LSM. Environment and Climate Change
55 Canada (ECCC) developed and operationally uses SVS for hydrological forecasting (Gaborit et al., 2017). By addressing the identified shortcomings in previous model evaluation efforts, we evaluated SVS's ability to simulate deep percolation using high-resolution data from a large, experimentally constructed plot (soil enclosure) in Southeastern Quebec, Canada. The plot was equipped with two pan lysimeters and a network of soil moisture and soil temperature sensors. We used an ensemble simulation strategy, accounting for uncertainties in forcing data and (a subset of) the model's soil hydraulic parameters. Our

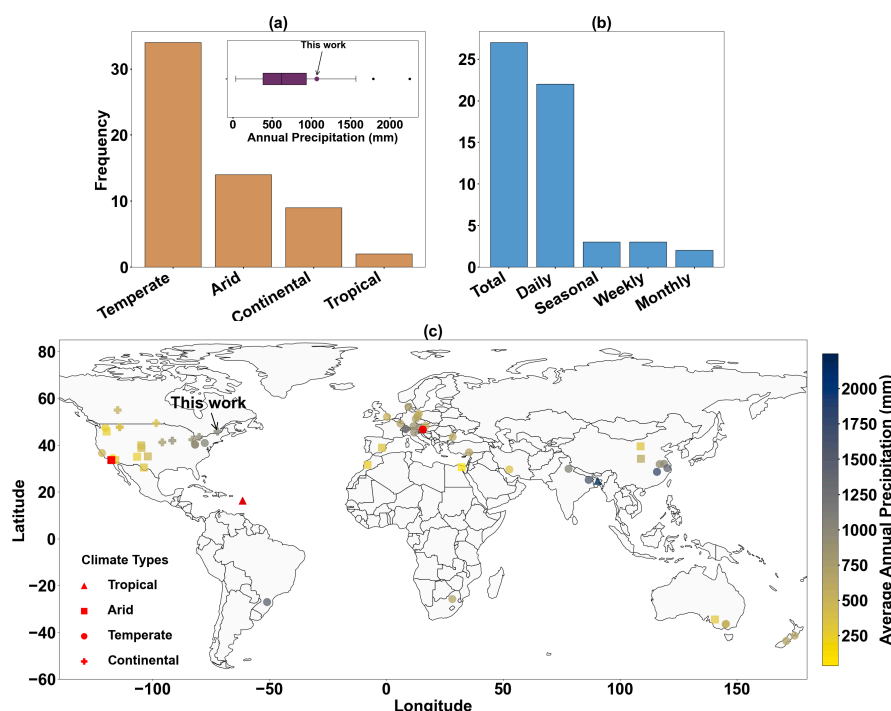


Figure 1. The distribution of climate types across the case studies within the reviewed works (a), including their range of average annual precipitation, and the frequency of temporal resolutions for evaluating deep percolation model outputs (b). Case study locations from the reviewed literature, distinguished by Köppen climate classification and average annual precipitation. Sites marked in red indicate missing precipitation data (c).

60 assessment explicitly accounted for uncertainties due to measurement errors and soil heterogeneity. The uncertainties were factored into the calculation of performance metrics. Additionally, we implemented a simple soil-freezing scheme for SVS, which is assessed for the first time in the scientific literature.

2 Case study

2.1 Experimental plots

65 Figure 2-d indicates the location of the experimental plot within the St-Nicéphore landfill site ('Study Site') in Drummondville, Quebec, Canada. An aerial view of the 280 m² plot post-construction is provided in Figure 2-a. Figure 2-b shows the plot one month after construction. The soil configuration and dimensions of the pan lysimeters, namely the L1 and L2 lysimeters, are illustrated in Figure 2-c. The lysimeters measured deep percolation hourly using tipping counters (KIPP-100, METER Group Inc.; 100 ml per tip). Soil water content and soil temperature are monitored half-hourly by dielectric sensors (METER Group Inc., 5TM), represented by blue dots in Figure 2-c. Figure 2-c shows the 15 cm topsoil layer atop the cover material (a sandy

70

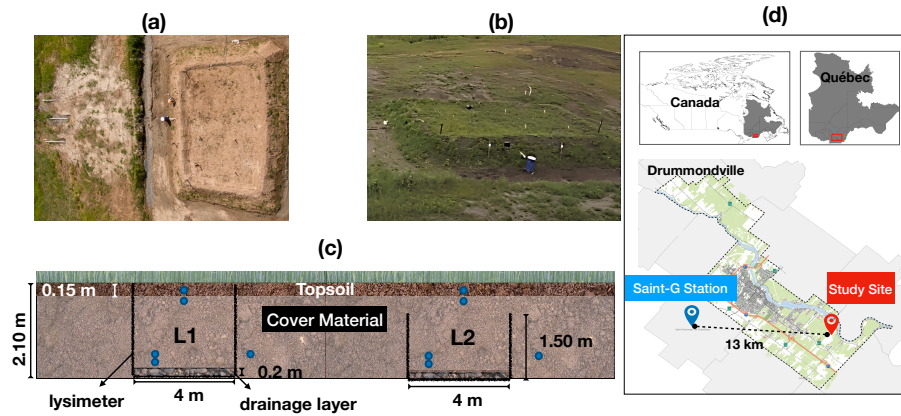


Figure 2. Experimental plot at the St-Nicéphore landfill. (a) Aerial view at completion. (b) Plot after one month. (c) Cross-section showing soil layers, pan lysimeters, and soil moisture/temperature sensors (blue dots at 75, 225, 1750, and 1850 mm depths). (d) Map showing the study site and the Saint-Germain-de-Grantham (Saint-G) weather station.

to silty soil commonly used as final cover at this landfill site). The configuration sits above a 20-cm sand-and-gravel drainage layer within each lysimeter. Table 1 outlines the properties of the topsoil and cover material. We used sieve and hydrometer analyses to determine sand and clay content. The soil's (vertical) saturated hydraulic conductivity (K_{sat}) was obtained using KSAT and Mini Disk Infiltrometer (Naik et al., 2019) devices (METER Group, Inc.). The soil water retention (SWR) model's empirical parameters, namely the air-entry suction and the slope of the SWR curve (ψ_{ae} , and b), were derived in the laboratory using the HYPROP (METER Group, Inc.) technique proposed by Schindler and Müller (2017); Schindler et al. (2015).

2.2 Data

The study site receives over 1050 mm of precipitation annually, with an average snowfall of 227 cm. Historically (1982–2017), the location experiences 109 days annually with more than 3 cm of snow on the ground. While we had two on-site weather stations, their data was unsuitable due to large gaps and a significant underestimation of precipitation. Therefore, the meteorological forcing for SVS was mainly obtained from the Saint-Germain-de-Grantham (Saint-G in Figure 2-d) weather station, located 13 km from the site. No elevation correction was applied since the station is roughly at the same elevation (85 m for Saint-G. and 110 m for our study site). Shortwave and longwave radiation fields, unavailable at the weather station, were sourced from the ERA5 reanalysis (Hersbach et al., 2020). We estimated specific humidity using the dew point temperature and atmospheric pressure. The Saint-Germain-de-Grantham station uses a double Alter Shield precipitation gauge. Precipitation measurements were adjusted for wind bias using the formula suggested by Kochendorfer et al. (2017). Rainfall and snowfall were distinguished using the equation proposed by Jennings et al. (2018) based on relative humidity and air temperature (Equation 1):



Soil Type	Parameter	N	Min	Max	Median	Ens-Min	Ens-Max
Topsoil	Sand (%)	6	37.0	92.0	75.0		
	Clay (%)	6	0.0	0.0	0.0		
	K_{sat} ($\text{m}\cdot\text{s}^{-1}$)	58	1.0×10^{-6}	2.1×10^{-4}	1.4×10^{-5}	5.1×10^{-7}	5.0×10^{-6}
	ψ_{ae} (m)	4	0.24	0.51	0.39	0.05	0.45
	b (-)	4	0.4	2.4	1.0	1.0	2.0
	θ_{sat} ($\text{m}^3\cdot\text{m}^{-3}$)					0.39	0.44
	θ_{fc} ($\text{m}^3\cdot\text{m}^{-3}$)					0.08	0.17
	θ_{unf} ($\text{m}^3\cdot\text{m}^{-3}$)					0.06	0.10
Cover M.	Sand (%)	5	55.0	78.0	68.0		
	Clay (%)	5	6.0	12.0	7.0		
	K_{sat} ($\text{m}\cdot\text{s}^{-1}$)	64	2.0×10^{-6}	1.3×10^{-4}	1.8×10^{-5}	1.0×10^{-6}	5.0×10^{-6}
	ψ_{ae} (m)	7	0.32	0.40	0.35	0.6	0.8
	b (-)	7	1.3	2.1	1.9	1.0	3.5
	θ_{sat} ($\text{m}^3\cdot\text{m}^{-3}$)					0.35	0.37
	θ_{fc} ($\text{m}^3\cdot\text{m}^{-3}$)					0.20	0.28
	θ_{unf} ($\text{m}^3\cdot\text{m}^{-3}$)					0.03	0.05

Table 1. Descriptive statistics of laboratory-estimated physical and hydraulic soil properties for topsoil and cover material. Parameters include percentages of sand and clay, saturated hydraulic conductivity (K_{sat}), saturated water content (θ_{sat}), field capacity (θ_{fc}), unfrozen residual water content (θ_{unf}), and the empirical parameters related to the soil water retention model: air-entry pressure (ψ_{ae}), and the b coefficient. 'Ens-Min' and 'Ens-Max' indicate parameter ranges for ensemble construction.

$$P_{snow} = \frac{1}{[1 + \exp c_1 + (c_2 T_a) + (c_3 R_h)]} \quad (1)$$

90 where T_a is air temperature ($^{\circ}\text{C}$), R_h is the relative humidity (%), and c_1, c_2, c_3 are empirical coefficients equal to -10.04, 1.41, and 0.09, respectively. Precipitation is recognized as snow if P_{snow} is greater than 0.5 and rain otherwise.

3 Methods

3.1 SVS land surface model

This study used the SVS land surface model, developed and maintained by ECCC (Alavi et al., 2016; Husain et al., 2016; Leonardini et al., 2021). SVS requires seven hourly meteorological inputs: air temperature, shortwave and longwave radiation, wind speed, specific humidity, atmospheric pressure, and precipitation. For snow-free conditions, initial values for soil moisture (volumetric liquid water content) and soil temperature within each model's soil layer must be provided. Information



about vegetation temperature and intercepted liquid water content is also required. SVS divides each grid cell into four tiling components: 1) bare ground; 2) low or high vegetation; 3) snow over bare ground and low vegetation; and 4) snow under high
100 vegetation. It uses a force-restore approach (Bhumralkar, 1975; Blackadar, 1976) for energy budget calculations and uses a one-layer representation of snow and vegetation canopy. A detailed overview of the SVS snow accumulation and melt routine can be found in Leonardini et al. (2021). The Richards equation governs vertical water movement in the soil, solved using a finite difference scheme (Verseghy, 1991). SVS uses Brooks and Corey's equations (Clapp and Hornberger, 1978; Brooks, 1965) to model soil water retention curve (SWRC) and vertical hydraulic conductivity (K_v):

$$105 \quad \theta = \theta_{sat} \left(\frac{\psi}{\psi_{ae}} \right)^{-b^{-1}} \quad (2)$$

and

$$K_v = K_{v,sat} \left[\frac{\theta}{\theta_{sat}} \right]^{2b+3} \quad (3)$$

where ψ is soil suction (m), θ_{sat} is soil moisture at saturation ($\text{m}^3 \cdot \text{m}^{-3}$), and $K_{v,sat}$ is the saturated vertical hydraulic conductivity of the soil (ms^{-1}). In Equations 2 and 3, b (unitless) and ψ_{ae} (m) are empirical parameters related to the slope of the
110 water retention curve and the air-entry-value suction, respectively. SVS, by default, calculates percolation at the bottom of the soil column only when the soil moisture exceeds field capacity. Surface runoff is simulated when the precipitation rate exceeds the first layer's $K_{v,sat}$ or when the soil pores are saturated with water. Notably, the current operational SVS version does not simulate soil freezing and thawing and its impact on infiltration (Alavi et al., 2016). We implemented a simple soil-freezing scheme based on the heat-conduction algorithm of Hayashi et al. (2007) to address this limitation. Appendix A describes this
115 scheme in detail.

3.2 Experiment design

The experimental plot was constructed in 2018. Due to the potential impact of plot stabilization, we excluded the first year of field data (deep percolation, soil temperature, and moisture) from the model's performance evaluation. Meteorological data from July 2018 to September 2019 is used for model spin-up, with simulations considered for evaluation running from
120 September 2019 to October 2022. To ensure a more accurate representation of processes at the near-surface and the base, the 190 cm soil column had a varying vertical discretization. The top and bottom 15 cm segments were divided into 2.5 cm layers, while the middle section used 5 cm layers (totaling 44 layers). The lower hydraulic boundary was set as a seepage face to simulate the capillary barrier effect at the cover material/drainage layer interface (Scanlon et al., 2002, 2005). Median sand and clay content values (Table 1) are assigned to each layer. An ensemble simulation strategy was used to address uncertainties
125 in model parameter values and meteorological data. Thirty different scenarios were constructed for each, resulting in a 900-member ensemble. Simulations were done using a developed Python wrapper (<https://github.com/Alireza-Amani/svspyed>) and the ECCC's high-performance computing (HPC) cluster.



3.3 Constructing the ensemble

3.3.1 Model parameters

130 We selected sampling intervals for six model parameters that influence the movement and storage of water in the soil column: saturated vertical hydraulic conductivity (k_{sat}), volumetric liquid water content at saturation (θ_{sat}) and field capacity (θ_{fc}), unfrozen residual water content (θ_{unf} , see A), ψ_{ae} , and the b coefficient (Equation 2). We used a combination of laboratory measurements, field observations, and inverse modelling to determine the sampling range for these parameters. Soil moisture observations during the winter of 2019 helped to establish the θ_{unf} range. The initial sampling ranges for k_{sat} , ψ_{ae} , and b 135 were informed by the laboratory measurements (Table 1), and for θ_{sat} by soil moisture measurements. For each perturbation scenario, we used suction threshold values ranging from 1.0 to 3.4 m (10 to 33 kPa) to determine θ_{fc} . For example, a specific combination of ψ_{ae} and b along with a randomly chosen suction value from this range would be used in Equation 2 to calculate θ_{fc} for that scenario. Following the definition of initial sampling intervals for the parameters (k_{sat} , θ_{sat} , θ_{fc} , ψ_{ae} , and b), we further refined the sampling ranges using inverse modeling. This process involved a five-dimensional grid search (a total of 140 10,000 different combinations) using soil moisture data from April to September 2019. For each combination, we calculated errors between hourly simulated and observed soil moisture from sensors in both soil types. The combinations with the lowest errors for each soil type helped refine the final sampling ranges. We chose this period because it followed the first winter, when freeze-thaw cycles likely impacted soil hydraulic properties. The final parameter ranges are indicated in Table 1 (under the 'Ens-Min' and 'Ens-Max' columns). Finally, Latin hypercube sampling (Loh, 1996) was used to create ensemble members, 145 ensuring a well-distributed sample across the parameter space.

3.3.2 Meteorological forcing

We constructed the 30 meteorological scenarios by randomly perturbing the input variables according to the approach suggested by Charrois et al. (2016). This approach ensures physically consistent temporal variations in the perturbed data. We used a first-order autoregressive (AR1) model to calculate the perturbations:

$$150 \quad P_t = \phi P_{t-1} + \epsilon_t \quad (4)$$

In Equation 4, P_t is the perturbation value at time t , ϕ is the parameter for the autoregressive model, and ϵ is a white noise process with zero mean and σ^2 variance. ϕ is obtained by fitting the AR1 model to the time series of each variable, and variance (σ^2) is computed using the standard deviation of the residuals between the variables from the Saint-Germain-de-Grantham station and the corresponding variables from the on-site measurements (average of two stations) following Equation

$$155 \quad 5. \quad \sigma^2 = \sigma_{res}(1 - \phi^2) \quad (5)$$



Different perturbations were applied depending on the variable: additive perturbations for air temperature, dew point temperature, wind speed, and atmospheric pressure, and multiplicative perturbations for shortwave radiation and relative humidity (limited to [0.8, 1.2] to avoid extremes), following Charrois et al. (2016). Longwave radiation values are perturbed within $\pm 25 \text{ (W}\cdot\text{m}^{-2})$ based on Raleigh et al. (2015). Rainfall is perturbed within $\pm 5 \%$, according to the World Meteorological Organization's recommended range of uncertainty for automatic tipping-counter rain gauges (Lanza et al., 2005; Colli et al., 2013). Finally, the precipitation phase was determined after the perturbations were applied to air temperature and relative humidity.

3.4 Performance Assessment

The performance of the SVS ensemble for simulating soil moisture, soil temperature, snow depth, and deep percolation was evaluated using the Continuous Ranked Probability Score (CRPS, Grit et al. (2006); Matheson and Winkler (1976)). We used the formulation proposed by Stein and Stoop (2022) which evaluates the distance between the simulation CDF (F) and the observation CDF (G) based on the following formulation (Baringhaus and Franz, 2004; Székely and Rizzo, 2005):

$$\int_{-\infty}^{+\infty} [F(x) - G(x)]^2 dx = \mathbb{E}_{X,Y}(|X - Y|) - \frac{1}{2}[\mathbb{E}_{X,X'}(|X - X'|) + \mathbb{E}_{Y,Y'}(|Y - Y'|)] \quad (6)$$

where $X, X' (Y, Y')$ represent independent copies of a random variable with a CDF given by $F(G)$. For a given time step, we can calculate the CRPS of the SVS ensemble by (Stein and Stoop, 2022):

$$CRPS(F_x, G_y) = \frac{1}{N} \frac{1}{M} \sum_{i=1}^M \sum_{j=1}^N |x_i - y_j| - \frac{1}{2M^2} \sum_{j=1}^M \sum_{k=1}^M |x_j - x_k| - \frac{1}{2N^2} \sum_{j=1}^N \sum_{k=1}^N |y_j - y_k| \quad (7)$$

where $x(j)$ with $j = 1, \dots, N$ corresponds to the simulated values for an ensemble with N members, and $y(i)$ with $i = 1, \dots, M$ corresponds to the observed values for an observation ensemble of size M . The observation ensembles for soil moisture and soil temperature took into account both potential sensor errors and variability due to soil heterogeneity. Two sensors at each depth within the experimental plot made the latter possible. The manufacturer-reported sensor accuracies are $\pm 0.03 \text{ m}^3\cdot\text{m}^{-3}$ and $\pm 1^\circ\text{C}$ for soil moisture and soil temperature measurements, respectively. To construct the ensembles for soil moisture and soil temperature at each depth, we randomly perturbed the nominal values of each sensor a total of 30 times using a uniform distribution, resulting in an ensemble of size 60. Similarly, we applied random perturbations within the reported accuracy of $\pm 1 \text{ cm}$ for snow depth observations, creating a 60-member ensemble. Regarding the calculation of CRPS concerning deep percolation, where both lysimeters provided deep percolation measurements, we used both values; if one lysimeter had missing data, only the available measurement was used. Additionally, to compare the ensemble mean of simulated and observed variables, we used Pearson's correlation coefficient and mean-bias-error (MBE). The MBE was calculated by subtracting the observations from the simulated values. The evaluation metrics were calculated for cold (from November to March) and warm months, allowing us to assess seasonal variations in model performance.



185 4 Results

4.1 Snow depth

Figure 3 compares the measured and simulated daily snow depth from SVS and the weather station across three periods. The shaded area shows the 95% confidence interval of the ensembles, with lines representing the ensemble mean. The vertically shaded areas highlight periods with potential rain-on-snow events. These periods (hours) are characterized by near- or above-zero ($^{\circ}\text{C}$) air temperature and non-zero precipitation. The rain-on-snow events are important as they can significantly impact snowpack properties (Cohen et al., 2015; Juras et al., 2017; McCabe et al., 2007). Manual snow measurements taken on 10 different days at two locations (one near the enclosure, shown as squares, and one elsewhere on the site) are included in Figure 3 for comparison. Each one of those 10 measurements is the average of 10 samples (SWE and snow depth) along a path, taken with a Federal snow sampler. The close agreement between the weather station data and the manual measurements near the enclosure (MBE of -1.6 cm) suggests a reasonable agreement between the two measurements. Figure 3 also shows that the spread of observations is relatively low compared to the SVS ensemble. This narrow spread is because the uncertainty we have considered in the observations was limited to the sensor's expected accuracy range. It did not include spatial variability, which can be significant, as indicated by the manual snow measurements in the figure.

Figure 3 reveals a significant overlap between the SVS and snow depth observation ensemble. This agreement is reflected in the overall CRPS of 2.5 cm for the combined periods. The correlation coefficient (r) between the ensemble means is high for November 2019 to April 2020 (0.94) and November 2020 to April 2021 (0.99), indicating close agreement between the simulated and observed snowpack evolution. However, the period between November 2021 and April 2022 shows a substantial overestimation of snow depth starting February 17, 2022. The snow depth for the SVS ensemble increases by 9 cm on average between February 17 and 18, while this increase is only 3 cm based on observations. This divergence greatly impacted the evaluation metrics. Before February 17th, r is 0.98 with a slight positive bias (MBE +1.5 cm). The overestimation coincides with a potential rain-on-snow event (February 17th), with temperature fluctuating above and below freezing and substantial precipitation (24.9 mm). This suggests that the overestimation was likely due to a misclassification of the precipitation phase within the SVS ensemble. Figure 3-c highlights that this issue adversely affected model performance during late winter, a critical period with substantial snowmelt. The calculated CRPS and correlation coefficient for March 2022 (8.3 cm and 0.94) are noticeably worse than those for March 2020 (3.1 cm, 0.98) and March 2021 (3.8 cm, 0.98).

4.2 Near-surface soil temperature and soil moisture

Figure 4 compares the simulated and observed daily soil temperatures at 75 mm depth, divided into two periods (Figure 4-a: from September 2019 to November 2020 and Figure 4-b: from November 2020 to November 2021) for clarity. The SVS model performs well in simulating near-surface soil temperature across the entire period, with a CRPS of 0.8 ($^{\circ}\text{C}$) and a slight cold bias (-1.2 $^{\circ}\text{C}$). The scatter plot in Figure 6-a further supports this, showing good performance during warm and cold months (from November to March). The low observed variability in soil temperature in Figure 4 reflects both the low spatial variability within the enclosure and the sensors' accuracy.

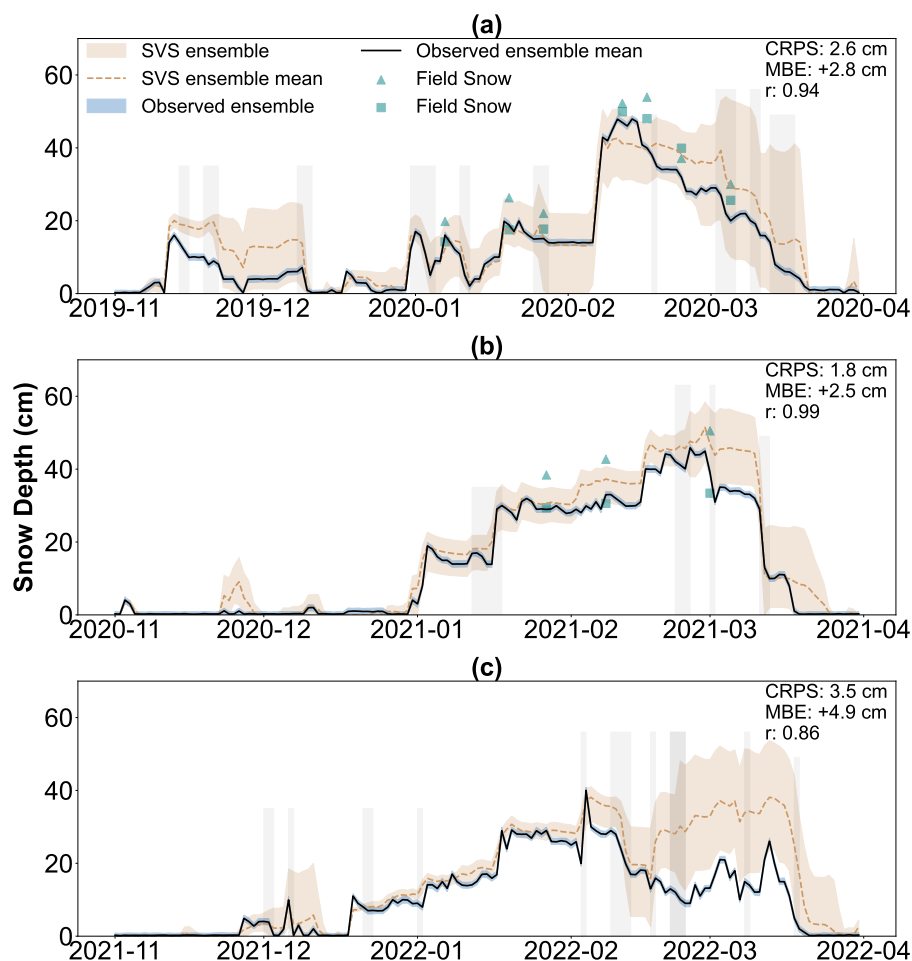


Figure 3. Daily snow depth (cm) for (a) November 2019 to April 2020, (b) November 2020 to April 2021, and (c) November 2021 to April 2022. The lines represent the ensemble mean of SVS and observation at the Saint-Germain-de-Grantham weather station, and the shaded area shows the 95 % confidence interval. The points represent manual snow measurements from two locations at the study site. The vertically shaded areas are indicators for periods with potential rain-on-snow events.

Figure 5 compares the simulated and observed daily soil moisture at 75 mm depth. The model exhibits acceptable agreement with observations for most of the period, with a CRPS of $0.02 \text{ m}^3 \cdot \text{m}^{-3}$. However, we observe a consistent pattern of under-estimation during February 2020, as well as January and February 2021. This issue is illustrated in Figure 6-b, with a bias of $-0.06 \text{ (m}^3 \cdot \text{m}^{-3})$ during cold months. During these periods, the SVS ensemble consistently assumed that the soil moisture was at the residual unfrozen water content due to the simulated soil freezing.

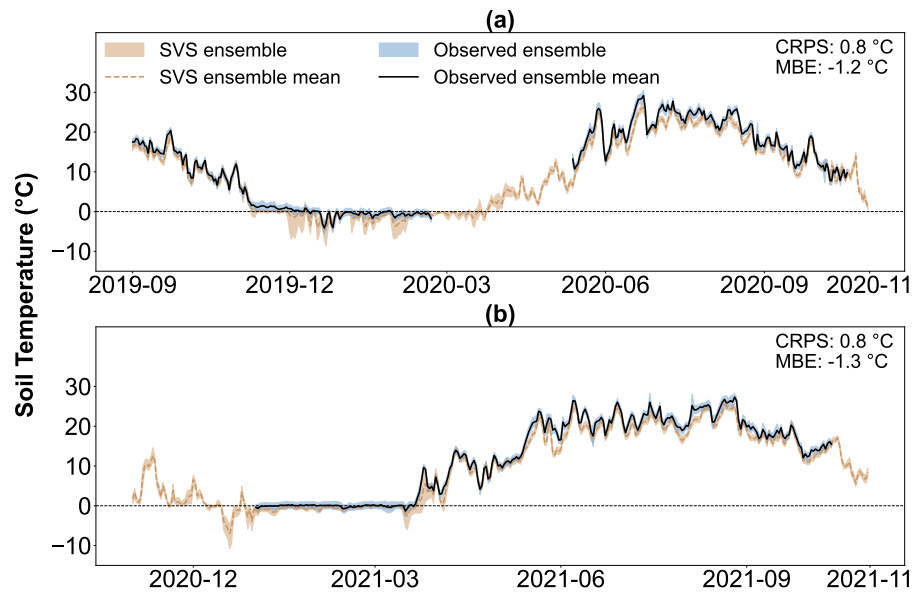


Figure 4. Daily averaged soil temperature at 75 mm ($^{\circ}\text{C}$) for (a) September 2019 to November 2020 and (b) November 2020 to November 2021. The lines represent the ensemble means of SVS and observation, and the shaded area represents the 95% confidence interval.

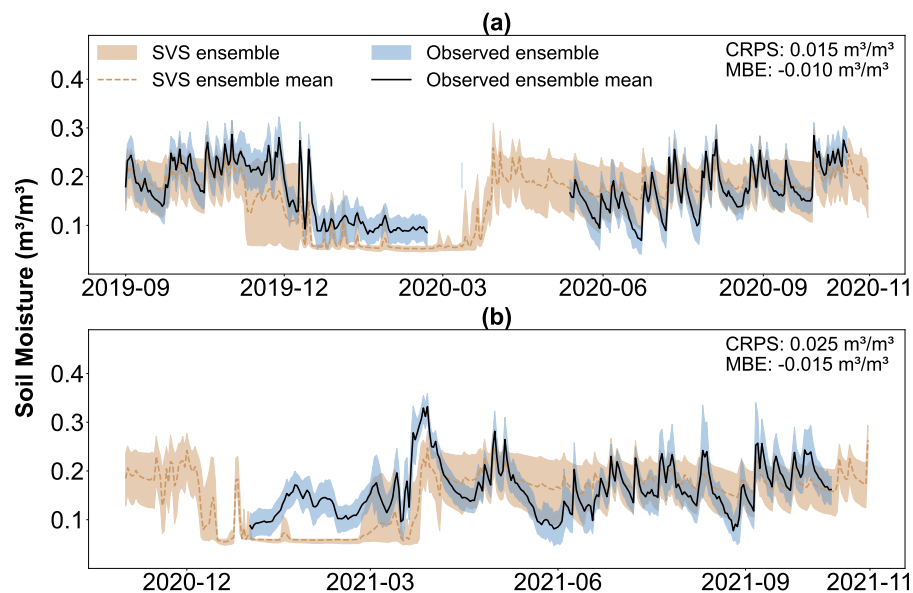


Figure 5. Daily averaged soil moisture at 75 mm (m^3m^{-3}) for (a) September 2019 to November 2020 and (b) November 2020 to November 2021. The lines represent the ensemble means of SVS and observation, and the shaded area represents the 95% confidence interval.

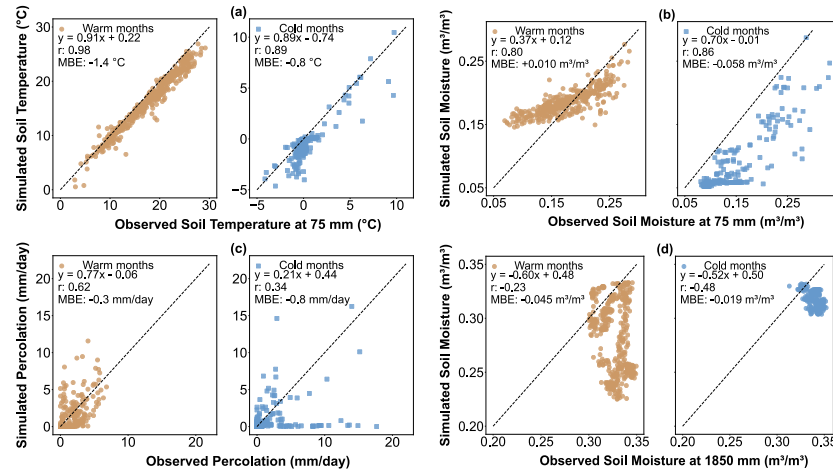


Figure 6. Scatter plot comparing daily simulated and observed ensemble means over the entire simulation period for (a) soil temperature at 75mm, (b) soil moisture at 75 mm, (c) deep percolation rates, and (d) soil moisture at 1850 mm below the surface.

4.3 Deep subsurface soil moisture

Figure 7 compares the simulated and observed daily soil moisture at 1850 mm depth, with Figure 6-d breaking down model performance by warm and cold months. From September 2019 to November 2020, the SVS ensemble closely matches the observations. This is reflected in the CRPS of $0.01 \text{ (m}^3 \cdot \text{m}^{-3})$. The model slightly underestimated (MBE: $-0.02 \text{ m}^3 \cdot \text{m}^{-3}$) soil moisture during this period, most notably during the summer of 2020. SVS maintained a good performance until the summer of 2021, where Figure 7-b visualizes a substantial divergence between the simulated and observed ensembles. This is reflected in the considerably worse CRPS ($0.04 \text{ m}^3 \cdot \text{m}^{-3}$) and MBE ($-0.05 \text{ m}^3 \cdot \text{m}^{-3}$) values for November 2020 to November 2021. Figure 6-d further emphasizes this underestimation bias during warm months. During cold months, however, Figure 6-d demonstrates a better performance for SVS with MBE equal to $-0.019 \text{ m}^3 \cdot \text{m}^{-3}$. Importantly, the negative correlation coefficients associated with cold and warm months may suggest a mismatch between the modelled and actual lower boundary conditions within the soil profile.

4.4 Deep percolation

Figure 8 compares the simulated and observed daily deep percolation rates from September 2019 to November 2022, with Figure 6-c further examining warm and cold months performances. Overall, SVS demonstrates a good agreement with observations, supported by CRPS values of $0.6 \text{ (mm} \cdot \text{day}^{-1})$ from September 2019 to November 2020, $0.2 \text{ (mm} \cdot \text{day}^{-1})$ from November 2020 to November 2021, and $0.8 \text{ (mm} \cdot \text{day}^{-1})$ from November 2021 to November 2022. The model captured the major percolation events reasonably well, including those driven by snowmelt (e.g., April 2020) and significant rainfall (e.g., 83.4 mm on August 3 and 4, and 50.3 mm on August 29, 2020). While there is a minor negative bias until November

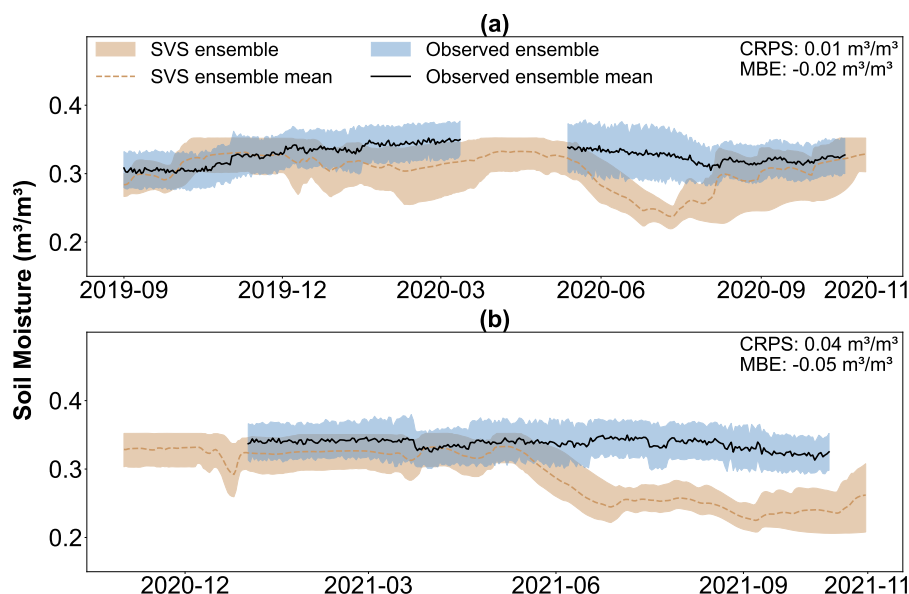


Figure 7. Daily averaged soil moisture at 1850 mm (m^3m^{-3}) for (a) September 2019 to November 2020 and (b) November 2020 to November 2021. The lines represent the ensemble means of SVS and observation, and the shaded area represents the 95% confidence interval.

2021 (MBE: $-0.2 \text{ mm}\cdot\text{day}^{-1}$), this underestimation increased significantly after November 2021 (MBE: $-1.5 \text{ mm}\cdot\text{day}^{-1}$). This change is largely attributed to SVS missing several deep percolation events during the winter of 2022, as also evident in Figure 6-c, where SVS simulates zero percolation on days with large observed values. This leads to a notably better performance during warm months (r : 0.62, MBE: $-0.3 \text{ mm}\cdot\text{day}^{-1}$) compared to colder months (r : 0.34, MBE: $-0.8 \text{ mm}\cdot\text{day}^{-1}$). It is worth noting that missing observations due to equipment issues impacted 36% of the days in the initial period (Sept. 2019–Nov. 2020).

5 Discussions

The results highlight the potential of SVS to simulate key hydrological processes influencing deep percolation. Yet, they also revealed important discrepancies with field data. These discrepancies raise questions such as: (i) Why is there a slight cold bias in near-surface soil temperature? (ii) What are the underlying reasons limiting the ability of the model to represent the dynamics of near-surface soil moisture during winter? (iii) What limits the model's ability to simulate subsurface soil moisture? (iv) How do these limitations influence deep percolation? In this section, we further investigate these questions.

5.1 Cold bias in SVS during snow-free conditions

A potential limitation within SVS is its underestimation of near-surface soil temperature during snow-free conditions with below-freezing air temperatures. This cold bias is evident in December 2019 and 2020 in Figure 4. This is likely due to the

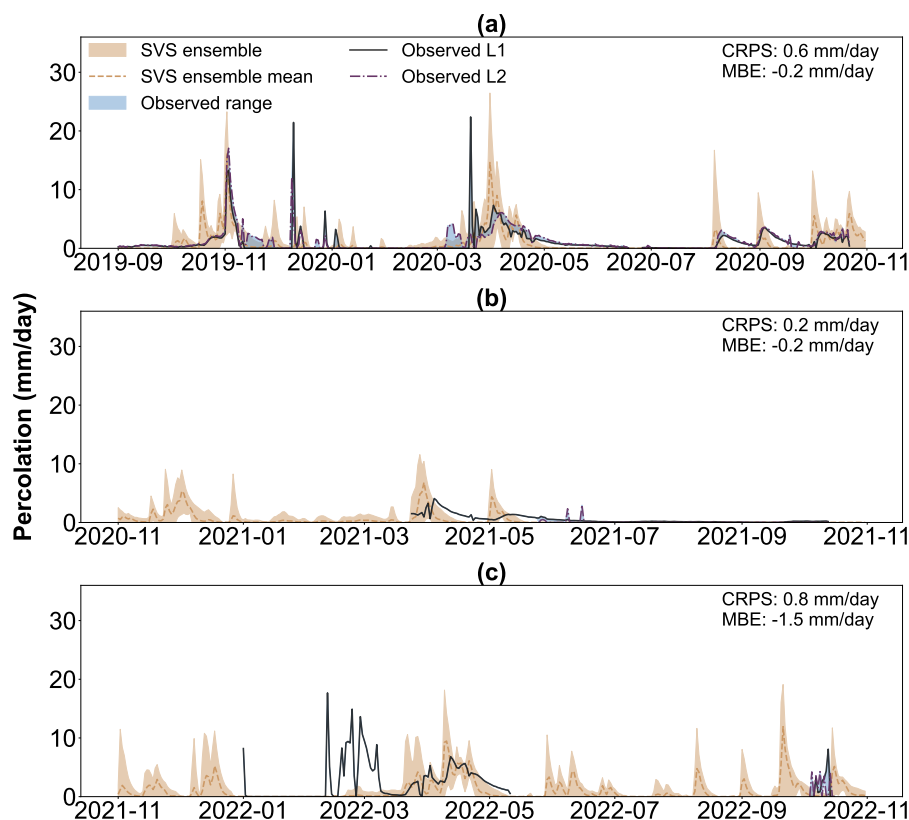


Figure 8. Daily deep percolation rates (mm day^{-1}) for (a) September 2019 to November 2020, (b) November 2020 to November 2021, and (c) November 2020 to November 2022. The lines represent the ensemble means of SVS and observations from the L1 and L2 lysimeters, and the shaded area represents the 95% confidence interval (SVS) and the range of two lysimeter observations.

model's simplified handling of soil temperature dynamics under such conditions. Currently, the soil freezing scheme in SVS uses as an upper boundary condition the surface temperature from a force-restore (FR) approach. The FR approach in SVS neglects the latent heat release that occurs during soil freezing and thawing (Husain et al., 2016), which can significantly impact soil temperature profiles. As shown by Boone et al. (2000), incorporating these latent heat effects into force-restore schemes leads to improved soil temperature simulations during freezing periods. Therefore, neglecting this aspect in SVS likely contributes to underestimating surface soil temperature in early winter snow-free conditions. This, in turn, affects the ground heat flux calculations used by the soil freezing scheme, potentially leading to an overestimation of frost depth.

5.2 Limitations of SVS in simulating soil moisture and deep percolation in winter

While potential limitations in SVS's soil freezing scheme exist, these may not fully explain the discrepancy in near-surface soil moisture during the winter of 2021 (Figure 5-b). Despite accurate soil temperature simulations (CRPS of $0.3\text{ }^{\circ}\text{C}$), soil moisture simulation significantly deviated in this period (CRPS of $0.05\text{ m}^3\cdot\text{m}^{-3}$). This highlights potential shortcomings in



representing hydrological processes under freezing conditions. Currently, SVS lacks the representation of water infiltration due to macropores in frozen soil, a complex process that can largely impact soil moisture dynamics (Watanabe et al., 2013; Jiang et al., 2020). This limitation is likely the main factor explaining the aforementioned discrepancy. It could also explain the missed deep percolation events during the winter of 2022 (Figure 8). In freezing conditions, snowmelt or rainfall can infiltrate and bypass frozen near-surface soil through preferential flow paths (macropores), directly reaching deeper soil layers (Demand et al., 2019; Watanabe and Kugisaki, 2017). Without accounting for this process, the model might underestimate deep percolation while overestimating surface runoff during freezing periods.

To further illustrate the model's limitations and their potential impacts, we examined a specific event in December 2019 (the 9th through the 12th) where SVS did not simulate deep percolation. Figure 9 presents the relevant data. Figure 9-a shows a likely rain-on-snow event with potentially considerable snowmelt infiltration during a warmer period. Figure 9-b reveals that the near-surface soil was likely frozen during the snowmelt event. It also indicates a good agreement between the simulated (ensemble mean) and observed (on top of the L2 lysimeter) soil temperatures. Interestingly, Figures 9-c and -d show that the infiltrated water bypassed the surface soil, directly reached the lysimeters (L2) base, and generated a significant deep percolation volume (18.2 mm). This hints at water movement through preferential flow paths. In contrast, the SVS model (ensemble mean) simulated no significant percolation and instead generated a considerable amount of surface runoff (29.2 mm).

5.3 Influence of Capillary Barrier on Simulated Subsurface Soil Moisture

Figure 6-d reveals a negative correlation coefficient between simulated and observed subsurface soil moisture (1850 mm) for both cold and warm months. This limitation in accurately simulating the dynamics of the soil moisture at the bottom of the soil column is potentially related to the choice of the lower hydraulic boundary condition in the model. We adopted a seepage face boundary condition as it is often suggested in studies involving lysimeters to approximate the capillary barrier effect induced by the inclusion of the drainage layer at the bottom of the lysimeters (Scanlon et al., 2002, 2005). The capillary barrier increases water storage in the finer layer situated just above, potentially keeping this finer layer close to saturation (Mancarella and Simeone, 2012; Abdolazadeh et al., 2011). Our results suggest that a more sophisticated boundary condition is required to more accurately reproduce the temporal variation of soil moisture close to a capillary barrier (Gao et al., 2023; Hübner et al., 2017; Kahale and Cabral, 2024). Despite the negative correlation, Figure 7 reveals that the simulated ensemble has a relatively high overlap with the observations during the cold months where the movement of water in the soil is predominantly downward, reflected in a small CRPS value of $0.007 \text{ m}^3 \cdot \text{m}^{-3}$. However, a notable underestimation occurs during warm months, particularly during the summers of 2020 and 2021, with CRPS equal to $0.036 \text{ (m}^3 \cdot \text{m}^{-3}\text{)}$, significantly worse than 0.007.

To further analyze the summertime underestimation, Figure 10 compares simulated (ensemble mean) and observed (sensors inside and outside the L1 lysimeter) soil moisture at different depths from May to September 2020. Figure 10-c reveals the underestimation becomes increasingly pronounced during the warmer months. Figure 10-b shows a similar, though less severe, underestimation at 1750 mm. Interestingly, the simulated soil moisture at 1750 mm agreed better with the sensor located outside ('ext' in Figure 10-b) the lysimeter, where no capillary barrier effect was present. The sensor's data revealed a drying pattern

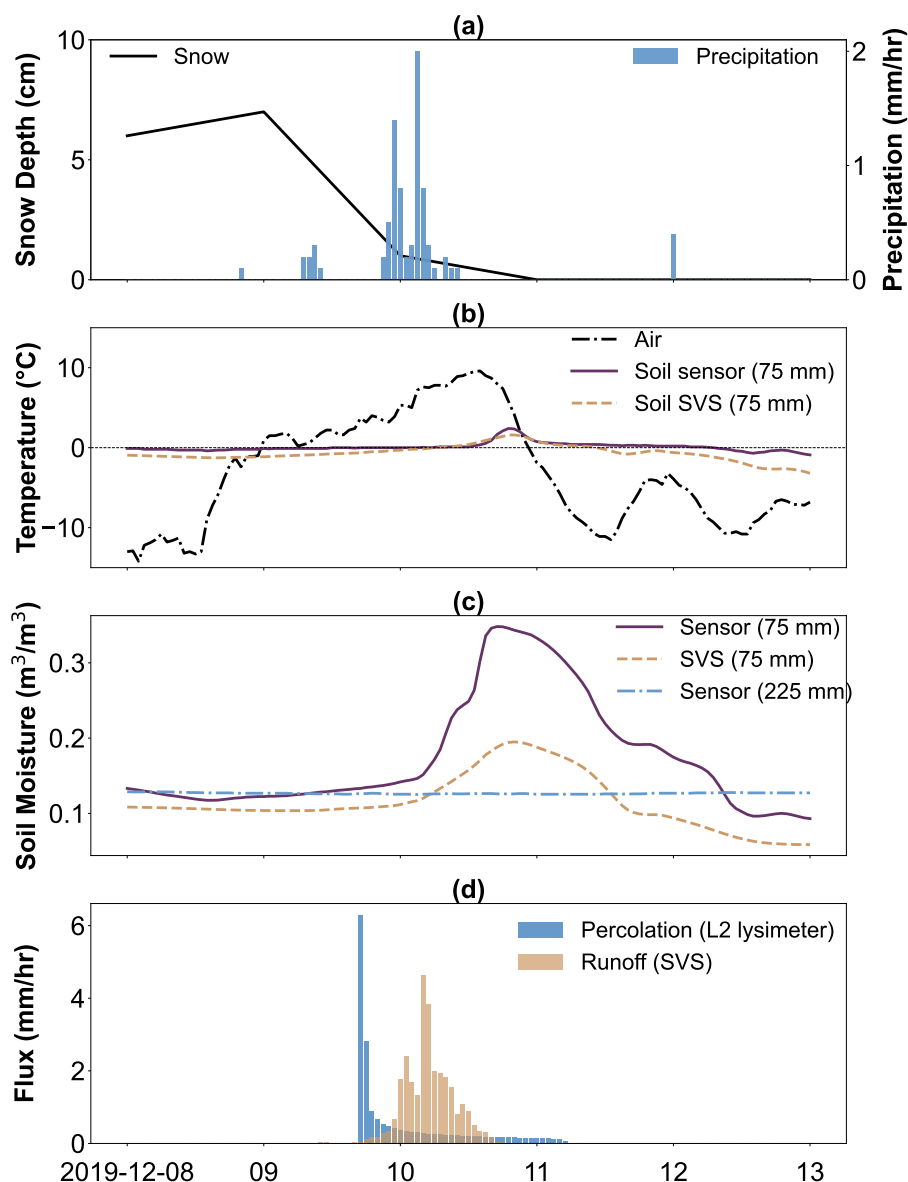


Figure 9. Time series (2019-12-09 to 2019-12-13) of (a) snow depth (cm) and precipitation (mm/hr), (b) air and soil temperature at 75mm below the surface (°C), (c) observed and simulated soil moisture at 75mm and 225mm below the surface (m^3/m^3), (d) percolation from the L2 lysimeter (mm/hr) and simulated surface runoff (mm/hr)

similar to the model, hinting at the influence of the lysimeter on the upward movement of water (the drying front) from deeper soil layers (Oldecop et al., 2017). This finding resonates with those of McCartney and Zornberg (2010), who investigated the zone of influence of a (geosynthetic) capillary barrier at the bottom of a laboratory-constructed 1350 mm soil column. During a three-month evaporation stage (using heat lamps), their soil moisture measurements did not show a significant decrease beyond

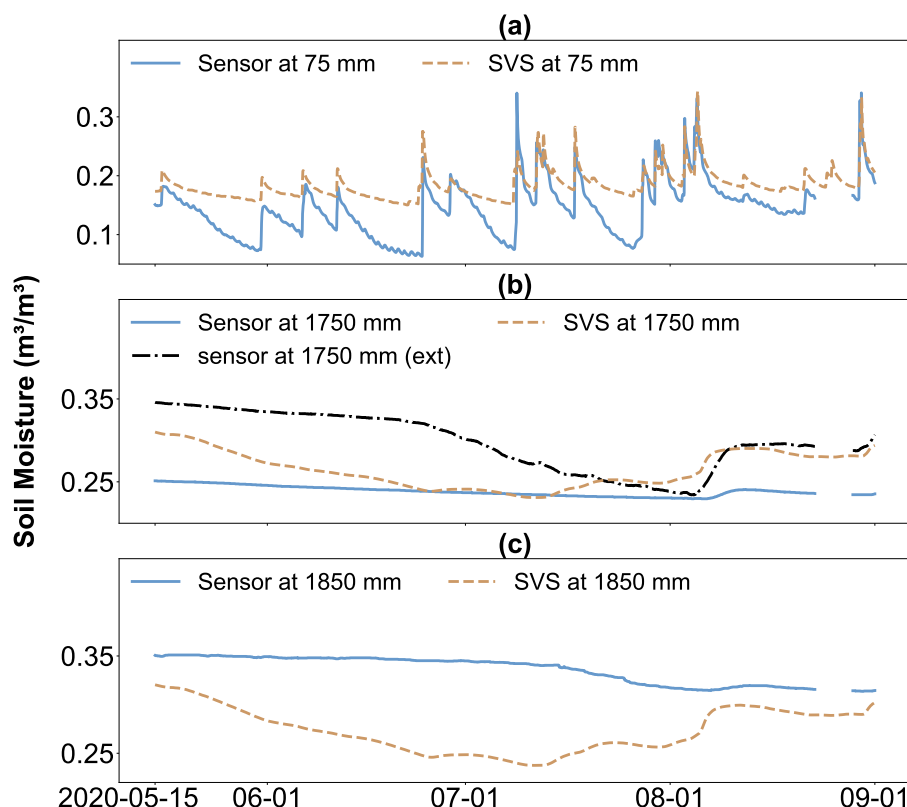


Figure 10. Time series (May 15–Sept. 1, 2020) of simulated (ensemble mean) and observed (the L1 lysimeter) daily soil moisture (m^3/m^3) at different depths (a) 75 mm, (b) 1750 mm, and (c) 1850 mm. Note: 'ext' indicates a soil moisture sensor outside the L1 lysimeter.

700 mm below the surface. In other words, the drying front only progressed 700 mm into the soil layer. This analysis raises important questions for future research. Could the lysimeter's influence explain the near-surface soil moisture disagreement in Figure 10-a? Did the capillary barrier alone, or other lysimeter characteristics (e.g., no-flux boundary walls), contribute to this effect? We also need more integrated data (deep percolation and soil moisture) during summer periods to fully evaluate the impact on deep percolation simulations.

6 Conclusions

Robust process-based evaluation of land surface models is critical for understanding and improving their ability to simulate deep percolation, particularly in cold regions where complex hydrological processes interact. Previous model evaluation studies often neglected the potential influence of uncertainties in forcing data, parameter values, and observations. Evaluations frequently relied on data with coarse temporal resolution and rarely included processes such as snow and soil freezing. This study aimed to address these critical gaps. We comprehensively evaluated the Soil, Vegetation, and Snow (SVS) land surface



model using high-resolution data from a large instrumented experimental plot built in the St-Nicéphore landfill site in south-eastern Quebec, Canada. Our performance assessment approach accounted for uncertainty in meteorological inputs, a subset of the model's hydraulic parameters, and observations. Furthermore, we evaluated a newly implemented soil freezing scheme implanted within the SVS model for the first time.

320 The results showed that the simulated and observed daily snow depth correlated well for most of the simulation period, with a correlation coefficient (r) greater than 0.94 and a mean-bias-error (MBE) smaller than 3.0 cm. This suggests a good representation of snow accumulation and ablation processes within SVS. The soil freezing scheme simulated near-surface daily soil temperature very well in cold months (r : 0.89), with a slight cold bias (MBE: $-0.8\text{ }^{\circ}\text{C}$) due to potential shortcomings in representing the latent heat exchange during freezing and thawing cycles. SVS showed promise in capturing deep percolation
325 events driven by spring snowmelt and heavy summer and fall rainfall events. However, the model struggled to simulate percolation events during cold months (r : 0.35) and under freezing conditions due to a lack of representation for infiltration in frozen soil and the influence of preferential flow pathways. These limitations also negatively impacted SVS's ability to simulate near-surface soil moisture during winter (MBE: $-0.058\text{ m}^3\cdot\text{m}^{-3}$).

Our findings underscore challenges and important considerations for accurately simulating cold-region deep percolation
330 dynamics. Future studies can focus on improving the representation of frozen soil infiltration and preferential flow pathways within SVS and potentially other land surface models. Prioritizing the collection and subsequent open-access sharing of long-term, high-resolution integrated field measurements can facilitate such model improvements. Expanding model evaluations to include other cold regions, longer periods, and diverse land covers is essential for developing robust cold region hydrological models. This approach can further improve deep percolation simulation by land surface models and enhance our understanding
335 of cold region hydrology and its response to a changing climate.

Data availability. The data presented in this study, including deep percolation, soil temperature, and moisture, and the laboratory measurements is included in an open repository accessible at Cabral et al. (2024).

Appendix A: Soil freezing module in SVS

SVS uses a hybrid approach that combines Force Restore schemes to compute the surface energy budget of bare ground, vegetation, and snow (Husain et al., 2016) with a multi-layer hydrological module solving the Richards equations for unsaturated
340 flow in a porous media (Alavi et al., 2016). This hybrid approach initially prevented the simulation of soil freezing and thawing by the model. To overcome this limitation, a new module has been developed.

The representation of soil freezing in SVS relies on the soil freezing/thawing module available in the Versatile Soil Budget Model (VSMB, Mohammed et al., 2013). This module is based on the simple heat-conduction algorithm of Hayashi et al.
345 (2007) and simulates the evolution of soil temperature and associated phase changes without the computationally expensive iterative solution of coupled non-linear equations. In SVS, soil temperature, and phase changes are solved on the same vertical



grid as the hydrological processes using upper boundary conditions provided by the force restore schemes solving the multiple energy budgets at the surface (Husain et al., 2016).

A1 Heat conduction algorithm

350 In the soil temperature algorithm, the heat conduction between two adjacent soil layers (upper to lower) is given by:

$$q_h = -\lambda_s \frac{\Delta_z T}{\Delta z} \quad (\text{A1})$$

where q_h is the soil heat flux (W m^{-2}), $\Delta_z T$ is the difference in soil temperature between adjacent layers (lower minus upper) (K), Δz is the distance between the centers of the layers (m) and λ_s is the bulk thermal conductivity given by the thickness-weighted harmonic mean conductivity of the two layers ($\text{W K}^{-1} \text{m}^{-1}$).

355 For a given soil layer j , the net heat flux ($\Delta_z q_{h,j}$) is then computed as:

$$\Delta_z q_{h,j} = q_{h,j-1} - q_{h,j} \quad (\text{A2})$$

The soil temperature algorithm assumes then that the change in net heat flux corresponds to a change in heat stored as sensible and latent heat in layer j :

$$\Delta_z q_{h,j} = (\Delta_t T_j c_{s,j} + \Delta_t w_{i,j} \rho_w L_f) d_j \quad (\text{A3})$$

360 where $\Delta_t T_j$ (K) and $\Delta_t w_{i,j}$ (kg kg^{-1}) are the changes in soil temperature and liquid equivalent ice content of layer j , respectively, with time, ρ_w is the density of water (kg m^{-3}), L_f is the latent heat of fusion (J kg^{-1}), d_j is the layer thickness (m), and $c_{s,j}$ is the volumetric heat capacity of the soil layer ($\text{J m}^{-3} \text{K}^{-1}$).

The VSMB soil freezing scheme assumes that water in soil pores freezes at $T_{ref} = 273.15 \text{ K}$ and ignores the freezing-point depression (Kurylyk and Watanabe, 2013). It accounts for the presence of unfrozen water that remains in the soil at sub-zero temperatures and co-exists with ice. The default VSMB algorithm assumes that the residual unfrozen water content, $w_{l,r}$, is constant and equals 0.06 by default. This option has been used in the work since it corresponds well to local observations of residual liquid water content in frozen conditions. Another option in SVS allows the unfrozen residual water content to depend on the soil texture based on Niu and Yang (2006). If a soil layer j is completely thawed or frozen with no liquid water above the residual frozen water content (i.e., $T_j \neq T_{ref}$), $\Delta_z q_{h,j}$ is converted to sensible heat until T_j reaches T_{ref} and any residual is converted to latent heat (melting of freezing). If the soil is already frozen ($T_j = T_{ref}$), $\Delta_z q_{h,j}$ is first used for phase change of all available liquid water above $w_{l,r}$ and any residual is converted to sensible heat. Calculations are performed sequentially from the top to the lowest soil layer.

365

370

The thermal heat capacity, c_s , and thermal conductivity, λ_s , of the soil layers are parameterized following Peters-Lidard et al. (1998) as functions of soil moisture and texture (percentage of sand and clay) and account for the effect frozen soils



375 as described in Boone et al. (2000). The dry soil thermal conductivity and soil thermal conductivity are taken from He et al. (2021) and Johansen (1975), respectively.

A2 Lower boundary condition

The heat flux at the bottom of the lowest soil layer is specified using an annual mean deep soil temperature, T_{btm} , and an appropriate scaling depth, z_{btm} . It is written as:

380
$$q_{h,N} = \lambda_{s,N} \frac{T_N - T_{btm}}{(z_{btm} - z_N)} \quad (A4)$$

where N corresponds to the deepest soil layer. In this study, T_{btm} was set to 7.5 (°C) and z_{btm} set to 5 m.

A3 Upper boundary condition

The upper boundary condition accounts for the surface tiling use in SVS. It includes contributions from: (i) snow-free bare ground, (ii) snow-free low and high vegetation, (iii) snow over bare ground and low vegetation, and (iv) snow below high
385 vegetation. The heat flux at the top of the superficial soil layer is written as:

$$q_{h,0} = f_{grnd} H_{grnd} + f_{veg} H_{veg} + f_{snw} H_{snw} + f_{snwv} H_{snwv} \quad (A5)$$

Where f_{grnd} and f_{veg} are the fractions of snow-free bare ground and snow-free low and high vegetation, respectively. f_{snw} and f_{snwv} represent the fraction of low vegetation and bare ground covered by snow and the fraction of soil under high vegetation covered by snow, respectively. H_{grnd} , H_{veg} , H_{snw} and H_{snwv} are the heat flux (W m^{-2}) from snow-free bare
390 ground, snow-free vegetation, snow over bare ground and low vegetation and snow below high vegetation.

For bare ground, the heat flux depends on the difference between the skin-temperature T_{gs} simulated by the force-restore approach for bare ground and the temperature of the upper soil layer ($j=1$). It is written as:

$$H_{grnd} = \frac{T_{gs} - T_1}{R_g} \text{ with } R_g = \frac{d_1}{2\lambda_{s,1}} \quad (A6)$$

In its current version, the soil freezing scheme has no feedback on the force restore scheme used for bare ground. Therefore,
395 the prognostic temperature variables of the force restore scheme used for bare ground lack the effect of latent heat release due to soil freezing and thawing. This can lead to an underestimation of soil temperature during soil freezing and an overestimation of soil temperature during soil thawing.

For snow-free low and high vegetation, SVS relies on the thermal coupling approach used in the EC-Land scheme (Boussetta et al., 2021). It uses the concept of skin conductivity to compute the heat exchanges between the vegetation tile and the soil.
400 The heat flux between the snow-free low and high vegetation and the upper soil layer is written as:

$$H_{veg} = (T_{vs} - T_1) \Lambda_v \quad (A7)$$

where T_{vs} is the vegetation skin temperature simulated by the force-restore approach and T_1 the temperature of the upper soil layer. Λ_v is the skin conductivity ($\text{W K}^{-1} \text{m}^{-2}$) for the vegetation. A first option in the code used a constant value of 10 W



$\text{K}^{-1} \text{m}^{-2}$ for low and high vegetation as in the default version of EC-Land (see Table 1.2 in the supplementary material of Boussetta et al. (2021)). A second option, used in this work, takes into account the effects of stable and unstable stratification as in Trigo et al. (2015).

The force restore schemes used for the snowpack over bare ground and low vegetation and the snowpack below high vegetation do not provide information on the temperature at the interface between the ground and the snow. Therefore, the deep snow temperature, $T_{snw,d}$, from the force restore scheme is used to estimate the heat flux between the superficial soil layer and the snow. It is written as:

$$H_{snw} = \frac{T_{snw,d} - T_1}{R_{snw}} \text{ with } R_{snw} = \frac{h_{therm}}{\lambda_{snw}} + \frac{d_1}{2\lambda_{s,1}} \quad (\text{A8})$$

where λ_{snw} is the snow thermal conductivity ($\text{W m}^{-1} \text{K}^{-1}$) and h_{therm} the thickness used to compute the thermal exchanges between the snowpack and the ground (m). h_{therm} depends on the snow damping depth, d_{snw} , used to characterize the diurnal variation of temperature close to the snow surface in the Force Restore scheme (Leonardini et al., 2021). h_{therm} is computed as $h_{therm} = \max(h_{snw}/2, h_{snw} - d_{snw})$ where h_{snw} is the total snow depth. The heat flux between the superficial soil layer and the snowpack below high vegetation, H_{snwv} , is derived in the same way as H_{snw} using the simulated information for the snowpack below high vegetation.

An accurate estimation of the fraction of the soil covered by snow is an important component of the soil freezing scheme. Indeed, it affects the estimation of the surface heat flux and strongly controls soil freezing in the fall and soil thawing in springtime. Two approaches can be used for snow cover fraction in the soil freezing scheme. For the first option, the fraction is computed as $f_{snw} = \max(1, \frac{\rho_{snw} h_{snw}}{W_{cr}})$ with $W_{cr} = 1 \text{ kg m}^{-2}$. The same formulation is used for f_{snwv} . With this formulation, the snow cover fraction reaches the value of 1 as soon as the snow is present on the ground. Such formulation is mainly suitable for point-scale applications of the soil freezing scheme and was used in the study. A second option, recommended for gridded simulations, relies on the formulation of Niu and Yang (2007):

$$f_{snw} = f_{snwv} = \tanh \left(\frac{h_{snw}}{2.5z_0 \left(\frac{\rho_{snw}}{\rho_{ref}} \right)^m} \right) \quad (\text{A9})$$

where $\rho_{ref} = 100 \text{ kg m}^{-3}$ and $m = 1.6$ are the default values from Niu and Yang (2007). In the soil freezing scheme, z_0 is set to 0.01 m to preserve a rapid increase of the snow cover fraction with snow depth. The term $\left(\frac{\rho_{snw}}{\rho_{ref}} \right)^m$ in the denominator aims at roughly representing the hysteresis associated with the snow cover fraction (Niu and Yang, 2007).

A4 Hydrological impact

The presence of frozen soil ($w_i > 0$) modifies the hydraulic conductivity at saturation and the soil porosity in the SVS soil hydrology scheme. The saturated hydraulic conductivity in the presence of frozen soil is written as $k_{satc} = f_{ice} k_{sat}$ where k_{sat} is the hydraulic conductivity at saturation that depends on soil texture. f_{ice} is a parameter that aims at reducing k_{sat} in presence of frozen water in the soil (e.g., Kurylyk and Watanabe, 2013). It is computed as in the CLASS land surface scheme



(Ganji et al., 2017):

$$f_{ice} = \left[1 - \max \left(0, \min \left(\frac{w_{sat} - 0.001}{w_{sat}}, \frac{w_i}{w_{sat}} \right) \right) \right]^2 \quad (A10)$$

where w_{sat} is the saturated volumetric water content.

The volumetric liquid water content at saturation is also reduced assuming that frozen water becomes part of the soil matrix (Zhao et al., 1997):

$$w_{satc} = \max(0.001, w_{sat} - w_i) \quad (A11)$$

440 Evapotranspiration is also indirectly impacted due to the change in the liquid water content when freezing and thawing occur.

Author contributions. Alireza Amani performed all the simulations and wrote the manuscript. Marie-Amélie Boucher guided the work and provided the general starting idea for the work (further improved by Alireza Amani), Alexandre Cabral planned and supervised the construction of the experimental plot. Vincent Vionnet and Étienne Gaborit provided the SVS model and guidance on this model. All authors contributed to analyzing the results and editing the manuscript.

445 *Competing interests.* The authors declare no conflicts of interest.

Acknowledgements. This study was partly supported by the Natural Science and Engineering Research Council of Canada (NSERC) grants RGPIN-2019-06455 (2nd author). This work was also supported by the Natural Sciences and Engineering Research Council of Canada grant CRD # RDPJ_508222-16 and the Consortium de recherche et innovations en bioprocédés industriels du Québec - (CRIBIQ) grant CRIBIQ_2017-014-C27 (3rd author)



450 References

- Abdollahzadeh, A. M., Lacroix Vachon, B., and Cabral, A. R.: Assessment of the design of an experimental cover with capillary barrier effect using 4 years of field data, *Geotechnical and Geological Engineering*, 29, 783–802, 2011.
- Alavi, N., Bélair, S., Fortin, V., Zhang, S., Husain, S. Z., Carrera, M. L., and Abrahamowicz, M.: Warm season evaluation of soil moisture prediction in the Soil, Vegetation, and Snow (SVS) scheme, *Journal of hydrometeorology*, 17, 2315–2332, 2016.
- 455 Arora, V. K., Seiler, C., Wang, L., and Kou-Giesbrecht, S.: Towards an ensemble-based evaluation of land surface models in light of uncertain forcings and observations, *Biogeosciences*, 20, 1313–1355, 2023.
- Baringhaus, L. and Franz, C.: On a new multivariate two-sample test, *Journal of multivariate analysis*, 88, 190–206, 2004.
- Benson, C., Abichou, T., Albright, W., Gee, G., and Roesler, A.: Field evaluation of alternative earthen final covers, *International Journal of Phytoremediation*, 3, 105–127, 2001.
- 460 Beven, K. and Young, P.: A guide to good practice in modeling semantics for authors and referees, *Water Resources Research*, 49, 5092–5098, 2013.
- Bhumralkar, C. M.: Numerical experiments on the computation of ground surface temperature in an atmospheric general circulation model, *Journal of Applied Meteorology and Climatology*, 14, 1246–1258, 1975.
- Blackadar, A. K.: Modeling the nocturnal boundary layer, in: *Preprints, Third Symp. on Atmospheric Turbulence, Diffusion, and Air Quality*, 465 Raleigh, Amer. Meteor. Soc., 1976.
- Boone, A., Masson, V., Meyers, T., and Noilhan, J.: The influence of the inclusion of soil freezing on simulations by a soil–vegetation–atmosphere transfer scheme, *Journal of Applied Meteorology and Climatology*, 39, 1544–1569, 2000.
- Boussetta, S., Balsamo, G., Arduini, G., Dutra, E., McNorton, J., Choulga, M., Agustí-Panareda, A., Beljaars, A., Wedi, N., Munõz-Sabater, J., et al.: ECLand: The ECMWF land surface modelling system, *Atmosphere*, 12, 723, 2021.
- 470 Brooks, R. H.: Hydraulic properties of porous media, Colorado State University, 1965.
- Cabral, A. R., Kahale, T., Ouédraogo, O., Duarte Neto, M., and Amani, A.: Integrated Lysimeter Study Data from Saint- Nicéphore, Quebec, <https://doi.org/10.5281/zenodo.10582140>, 2024.
- Cao, G., Scanlon, B. R., Han, D., and Zheng, C.: Impacts of thickening unsaturated zone on groundwater recharge in the North China Plain, *Journal of hydrology*, 537, 260–270, 2016.
- 475 Charrois, L., Cosme, E., Dumont, M., Lafaysse, M., Morin, S., Libois, Q., and Picard, G.: On the assimilation of optical reflectances and snow depth observations into a detailed snowpack model, *The Cryosphere*, 10, 1021–1038, 2016.
- Clapp, R. B. and Hornberger, G. M.: Empirical equations for some soil hydraulic properties, *Water resources research*, 14, 601–604, 1978.
- Cohen, J., Ye, H., and Jones, J.: Trends and variability in rain-on-snow events, *Geophysical Research Letters*, 42, 7115–7122, 2015.
- Colli, M., Lanza, L., and Chan, P.: Co-located tipping-bucket and optical drop counter RI measurements and a simulated correction algorithm, 480 *Atmospheric Research*, 119, 3–12, 2013.
- Cordeiro, M. R., Wilson, H. F., Vanrobaeys, J., Pomeroy, J. W., Fang, X., et al.: Simulating cold-region hydrology in an intensively drained agricultural watershed in Manitoba, Canada, using the Cold Regions Hydrological Model, *Hydrology and Earth System Sciences*, 21, 3483–3506, 2017.
- Dalin, C., Wada, Y., Kastner, T., and Puma, M. J.: Groundwater depletion embedded in international food trade, *Nature*, 543, 700–704, 2017.
- 485 Dash, C. J., Sarangi, A., Singh, D., and Adhikary, P.: Numerical simulation to assess potential groundwater recharge and net groundwater use in a semi-arid region, *Environmental monitoring and assessment*, 191, 371, 2019.



- Demand, D., Selker, J. S., and Weiler, M.: Influences of macropores on infiltration into seasonally frozen soil, *Vadose Zone Journal*, 18, 1–14, 2019.
- Fayer, M. J.: UNSAT-H version 3.0: Unsaturated soil water and heat flow model theory, user manual, and examples, Tech. rep., Pacific Northwest National Lab.(PNNL), Richland, WA (United States), 2000.
- 490 Fisher, R. A. and Koven, C. D.: Perspectives on the future of land surface models and the challenges of representing complex terrestrial systems, *Journal of Advances in Modeling Earth Systems*, 12, e2018MS001 453, 2020.
- Gaborit, É., Fortin, V., Xu, X., Seglenieks, F., Tolson, B., Fry, L. M., Hunter, T., Ancil, F., and Gronewold, A. D.: A hydrological prediction system based on the SVS land-surface scheme: Efficient calibration of GEM-Hydro for streamflow simulation over the Lake Ontario
- 495 basin, *Hydrology and Earth System Sciences*, 21, 4825–4839, 2017.
- Ganji, A., Sushama, L., Versegny, D., and Harvey, R.: On improving cold region hydrological processes in the Canadian Land Surface Scheme, *Theoretical and Applied Climatology*, 127, 45–59, 2017.
- Gao, C., Ye, W.-M., Lu, P.-H., Liu, Z.-R., Wang, Q., and Chen, Y.-G.: An infiltration model for inclined covers with consideration of capillary barrier effect, *Engineering Geology*, 326, 107 318, 2023.
- 500 Gleeson, T., Wada, Y., Bierkens, M. F., and Van Beek, L. P.: Water balance of global aquifers revealed by groundwater footprint, *Nature*, 488, 197–200, 2012.
- Graham, S. L., Srinivasan, M., Faulkner, N., and Carrick, S.: Soil hydraulic modeling outcomes with four parameterization methods: Comparing soil description and inverse estimation approaches, *Vadose Zone Journal*, 17, 1–10, 2018.
- Grimit, E. P., Gneiting, T., Berrocal, V. J., and Johnson, N. A.: The continuous ranked probability score for circular variables and its application to mesoscale forecast ensemble verification, *Quarterly Journal of the Royal Meteorological Society: A journal of the atmospheric sciences, applied meteorology and physical oceanography*, 132, 2925–2942, 2006.
- 505 Hayashi, M., Goeller, N., Quinton, W. L., and Wright, N.: A simple heat-conduction method for simulating the frost-table depth in hydrological models, *Hydrological Processes: An International Journal*, 21, 2610–2622, 2007.
- He, H., Liu, L., Dyck, M., Si, B., and Lv, J.: Modelling dry soil thermal conductivity, *Soil and Tillage Research*, 213, 105 093, 2021.
- 510 Hersbach, H., Bell, B., Berrisford, P., Hirahara, S., Horányi, A., Muñoz-Sabater, J., Nicolas, J., Peubey, C., Radu, R., Schepers, D., et al.: The ERA5 global reanalysis, *Quarterly Journal of the Royal Meteorological Society*, 146, 1999–2049, 2020.
- Ho, C. K., Arnold, B. W., Cochran, J. R., Taira, R. Y., and Pelton, M. A.: A probabilistic model and software tool for evaluating the long-term performance of landfill covers, *Environmental Modelling & Software*, 19, 63–88, 2004.
- Huang, F., Zhang, Y., Zhang, D., and Chen, X.: Environmental groundwater depth for groundwater-dependent terrestrial ecosystems in arid/semiarid regions: A review, *International journal of environmental research and public health*, 16, 763, 2019.
- 515 Hübner, R., Günther, T., Heller, K., Noell, U., and Kleber, A.: Impacts of a capillary barrier on infiltration and subsurface stormflow in layered slope deposits monitored with 3-D ERT and hydrometric measurements, *Hydrology and Earth System Sciences*, 21, 5181–5199, 2017.
- Husain, S. Z., Alavi, N., Bélair, S., Carrera, M., Zhang, S., Fortin, V., Abrahamowicz, M., and Gauthier, N.: The multibudget Soil, Vegetation, and Snow (SVS) scheme for land surface parameterization: Offline warm season evaluation, *Journal of Hydrometeorology*, 17, 2293–2313, 2016.
- 520 Jennings, K. S., Winchell, T. S., Livneh, B., and Molotch, N. P.: Spatial variation of the rain–snow temperature threshold across the Northern Hemisphere, *Nature communications*, 9, 1–9, 2018.



- Jiang, R., Li, T., Liu, D., Fu, Q., Hou, R., Li, Q., Cui, S., and Li, M.: Soil infiltration characteristics and pore distribution under freezing-thawing conditions, *The Cryosphere Discussions*, 2020, 1–31, 2020.
- Johansen, O.: Varmeledningsevne av jordarter (Thermal conductivity of soils), CRREL Draft English Translation, 637, 1975.
- Juras, R., Würzer, S., Pavlásek, J., Vitvar, T., and Jonas, T.: Rainwater propagation through snowpack during rain-on-snow sprinkling experiments under different snow conditions, *Hydrology and Earth System Sciences*, 21, 4973–4987, 2017.
- Kahale, T. and Cabral, A. R.: Field and numerical evaluation of breakthrough suction effects in lysimeter design, *Environmental Technology*, 45, 1169–1182, 2024.
- Khire, M. V., Benson, C. H., and Bosscher, P. J.: Water balance modeling of earthen final covers, *Journal of geotechnical and geoenvironmental engineering*, 123, 744–754, 1997.
- Kochendorfer, J., Rasmussen, R., Wolff, M., Baker, B., Hall, M. E., Meyers, T., Landolt, S., Jachcik, A., Isaksen, K., Brækkan, R., et al.: The quantification and correction of wind-induced precipitation measurement errors, *Hydrology and Earth System Sciences*, 21, 1973–1989, 2017.
- Kurylyk, B. L. and Watanabe, K.: The mathematical representation of freezing and thawing processes in variably-saturated, non-deformable soils, *Advances in Water Resources*, 60, 160–177, 2013.
- Lanza, L., Leroy, M., Alexandropoulos, C., Stagi, L., and Wauben, W.: Laboratory intercomparison of rainfall intensity gauges, *World Meteorological Organisation–Instruments and Observing Methods Rep*, 84, 2005.
- Leonardini, G., Ancil, F., Vionnet, V., Abrahamowicz, M., Nadeau, D. F., and Fortin, V.: Evaluation of the Snow Cover in the Soil, Vegetation, and Snow (SVS) Land Surface Model, *Journal of Hydrometeorology*, <https://doi.org/10.1175/jhm-d-20-0249.1>, 2021.
- Li, D. and Shao, M.: Temporal stability analysis for estimating spatial mean soil water storage and deep percolation in irrigated maize crops, *Agricultural Water Management*, 144, 140–149, 2014.
- Loh, W.-L.: On Latin hypercube sampling, *The annals of statistics*, 24, 2058–2080, 1996.
- Mancarella, D. and Simeone, V.: Capillary barrier effects in unsaturated layered soils, with special reference to the pyroclastic veneer of the Pizzo d’Alvano, Campania, Italy, *Bulletin of Engineering Geology and the Environment*, 71, 791–801, 2012.
- Matheson, J. E. and Winkler, R. L.: Scoring rules for continuous probability distributions, *Management science*, 22, 1087–1096, 1976.
- McCabe, G. J., Clark, M. P., and Hay, L. E.: Rain-on-snow events in the western United States, *Bulletin of the American Meteorological Society*, 88, 319–328, 2007.
- McCartney, J. S. and Zornberg, J. G.: Effects of infiltration and evaporation on geosynthetic capillary barrier performance, *Canadian Geotechnical Journal*, 47, 1201–1213, 2010.
- Meissner, R., Rupp, H., and Seyfarth, M.: Advances in out door lysimeter techniques, *Water, Air, & Soil Pollution: Focus*, 8, 217–225, 2008.
- Mijares, R. G. and Khire, M. V.: Field data and numerical modeling of water balance of lysimeter versus actual earthen cap, *Journal of geotechnical and geoenvironmental engineering*, 138, 889–897, 2012.
- Mohammed, G. A., Hayashi, M., Farrow, C. R., and Takano, Y.: Improved characterization of frozen soil processes in the Versatile Soil Moisture Budget model, *Canadian Journal of Soil Science*, 93, 511–531, 2013.
- Mölders, N., Haferkorn, U., Döring, J., and Kramm, G.: Long-term investigations on the water budget quantities predicted by the hydrothermodynamic soil vegetation scheme (HTSVS)–Part II: Evaluation, sensitivity, and uncertainty, *Meteorology and atmospheric physics*, 84, 137–156, 2003.
- Naik, A. P., Ghosh, B., and Pekkat, S.: Estimating soil hydraulic properties using mini disk infiltrometer, *ISH Journal of Hydraulic Engineering*, 25, 62–70, 2019.



- Niu, G.-Y. and Yang, Z.-L.: Effects of frozen soil on snowmelt runoff and soil water storage at a continental scale, *Journal of Hydrometeorology*, 7, 937–952, 2006.
- Niu, G.-Y. and Yang, Z.-L.: An observation-based formulation of snow cover fraction and its evaluation over large North American river
565 basins, *Journal of geophysical research: Atmospheres*, 112, 2007.
- Noori, R., Maghrebi, M., Jessen, S., Bateni, S. M., Heggy, E., Javadi, S., Noury, M., Pistre, S., Abolfathi, S., and AghaKouchak, A.: Decline in Iran's groundwater recharge, *Nature Communications*, 14, 6674, 2023.
- Nygren, M., Giese, M., and Barthel, R.: Recent trends in hydroclimate and groundwater levels in a region with seasonal frost cover, *Journal of Hydrology*, 602, 126 732, 2021.
- 570 Ogorzalek, A., Bohnhoff, G., Shackelford, C., Benson, C., and Apiwantragoon, P.: Comparison of field data and water-balance predictions for a capillary barrier cover, *Journal of geotechnical and geoenvironmental engineering*, 134, 470–486, 2008.
- Oldecop, L. A., Rodari, G. J., and Muñoz, J. J.: Atmosphere interaction and capillary barrier in filtered tailings, *Geotechnical and Geological Engineering*, 35, 1803–1817, 2017.
- Orellana, F., Verma, P., Loheide, S. P., and Daly, E.: Monitoring and modeling water-vegetation interactions in groundwater-dependent
575 ecosystems, *Reviews of Geophysics*, 50, 2012.
- Oreskes, N., Shrader-Frechette, K., and Belitz, K.: Verification, validation, and confirmation of numerical models in the earth sciences, *Science*, 263, 641–646, 1994.
- Ouédraogo, O., Duarte, M., Kahale, T., Abichou, T., and Cabral, A.: Parametric analysis of the efficacy of lysimeter designs using numerical modelling, *Geotechnical and Geological Engineering*, 40, 5361–5375, 2022.
- 580 Peel, M. C., Finlayson, B. L., and McMahon, T. A.: Updated world map of the Köppen-Geiger climate classification, *Hydrology and earth system sciences*, 11, 1633–1644, 2007.
- Peters-Lidard, C., Blackburn, E., Liang, X., and Wood, E. F.: The effect of soil thermal conductivity parameterization on surface energy fluxes and temperatures, *Journal of the Atmospheric Sciences*, 55, 1209–1224, 1998.
- Pomeroy, J., Brown, T., Fang, X., Shook, K. R., Pradhananga, D., Armstrong, R., Harder, P., Marsh, C., Costa, D., Krogh, S., et al.: The cold
585 regions hydrological modelling platform for hydrological diagnosis and prediction based on process understanding, *Journal of Hydrology*, 615, 128 711, 2022.
- Raleigh, M., Lundquist, J., and Clark, M.: Exploring the impact of forcing error characteristics on physically based snow simulations within a global sensitivity analysis framework, *Hydrology and Earth System Sciences*, 19, 3153–3179, 2015.
- Scanlon, B. R., Christman, M., Reedy, R. C., Porro, I., Simunek, J., and Flerchinger, G. N.: Intercode comparisons for simulating water
590 balance of surficial sediments in semiarid regions, *Water Resources Research*, 38, 59–1, 2002.
- Scanlon, B. R., Reedy, R. C., Keese, K. E., and Dwyer, S. F.: Evaluation of evapotranspirative covers for waste containment in arid and semiarid regions in the southwestern USA, *Vadose Zone Journal*, 4, 55–71, 2005.
- Schindler, U., von Unold, G., Durner, W., and Mueller, L.: Recent progress in measuring soil hydraulic properties, in: *Proceedings of the International Conference on Environment and Civil Engineering*, pp. 24–25, 2015.
- 595 Schindler, U. G. and Müller, L.: Soil hydraulic functions of international soils measured with the Extended Evaporation Method (EEM) and the HYPROP device, *Open Data Journal for Agricultural Research*, 3, 2017.
- Schwemmler, R. and Weiler, M.: Consistent modeling of transport processes and travel times—coupling soil hydrologic processes with StorAge Selection functions, *Water Resources Research*, 60, e2023WR034 441, 2024.



- Selim, T., Elkefay, S. M., Berndtsson, R., Elkiki, M., and El-Kharbotly, A. A.: Heavy Metal Transport in Different Drip-Irrigated Soil Types with Potato Crop, *Sustainability*, 15, 10 542, 2023.
- Simunek, J., Van Genuchten, M. T., and Sejna, M.: The HYDRUS-1D software package for simulating the one-dimensional movement of water, heat, and multiple solutes in variably-saturated media, *University of California-Riverside Research Reports*, 3, 1–240, 2005.
- Sobaga, A., Decharme, B., Habets, F., Delire, C., Enjelvin, N., Redon, P.-O., Faure-Cattelain, P., and Le Moigne, P.: Assessment of the interactions between soil–biosphere–atmosphere (ISBA) land surface model soil hydrology, using four closed-form soil water relationships and several lysimeters, *Hydrology and Earth System Sciences*, 27, 2437–2461, 2023.
- Stein, J. and Stoop, F.: Neighborhood-based ensemble evaluation using the CRPS, *Monthly Weather Review*, 150, 1901–1914, 2022.
- Stumpp, C., Stichler, W., Kandolf, M., and Simunek, J.: Effects of Land Cover and Fertilization Method on Water Flow and Solute Transport in Five Lysimeters: A Long-Term Study Using Stable Water Isotopes, *Vadose Zone Journal*, 11, 0, <https://doi.org/10.2136/vzj2011.0075>, 2012.
- Székel, G. J. and Rizzo, M. L.: A new test for multivariate normality, *Journal of Multivariate Analysis*, 93, 58–80, 2005.
- Trenberth, K. E.: Changes in precipitation with climate change, *Climate research*, 47, 123–138, 2011.
- Trigo, I., Boussetta, S., Viterbo, P., Balsamo, G., Beljaars, A., and Sandu, I.: Comparison of model land skin temperature with remotely sensed estimates and assessment of surface-atmosphere coupling, *Journal of Geophysical Research: Atmospheres*, 120, 12–096, 2015.
- Verseghy, D. L.: CLASS—A Canadian land surface scheme for GCMs. I. Soil model, *International Journal of Climatology*, 11, 111–133, 1991.
- Wada, Y., Van Beek, L. P., Van Kempen, C. M., Reckman, J. W., Vasak, S., and Bierkens, M. F.: Global depletion of groundwater resources, *Geophysical research letters*, 37, 2010.
- Watanabe, K. and Kugisaki, Y.: Effect of macropores on soil freezing and thawing with infiltration, *Hydrological Processes*, 31, 270–278, 2017.
- Watanabe, K., Kito, T., Dun, S., Wu, J. Q., Greer, R. C., and Flury, M.: Water infiltration into a frozen soil with simultaneous melting of the frozen layer, *Vadose Zone Journal*, 12, vzj2011–0188, 2013.
- Wheater, H. S., Pomeroy, J. W., Pietroniro, A., Davison, B., Elshamy, M., Yassin, F., Rokaya, P., Fayad, A., Tesemma, Z., Princz, D., et al.: Advances in modelling large river basins in cold regions with Modélisation Environnementale Communautaire—Surface and Hydrology (MESH), the Canadian hydrological land surface scheme, *Hydrological Processes*, 36, e14 557, 2022.
- Willcox, K. E., Ghattas, O., and Heimbach, P.: The imperative of physics-based modeling and inverse theory in computational science, *Nature Computational Science*, 1, 166–168, 2021.
- Wilson, C., Guivarch, C., Kriegler, E., Van Ruijven, B., Van Vuuren, D. P., Krey, V., Schwanitz, V. J., and Thompson, E. L.: Evaluating process-based integrated assessment models of climate change mitigation, *Climatic Change*, 166, 1–22, 2021.
- Wu, W.-Y., Lo, M.-H., Wada, Y., Famiglietti, J. S., Reager, J. T., Yeh, P. J.-F., Ducharme, A., and Yang, Z.-L.: Divergent effects of climate change on future groundwater availability in key mid-latitude aquifers, *Nature communications*, 11, 3710, 2020.
- Zhao, L., Gray, D. M., and Male, D. H.: Numerical analysis of simultaneous heat and mass transfer during infiltration into frozen ground, *Journal of Hydrology*, 200, 345–363, 1997.